JOURNAL OF GEOPHYSICAL RESEARCH, VOL. 114, B04103, doi:10.1029/2008JB006106, 2009



# Integrated archeomagnetic and micro–Raman spectroscopy study of pre-Columbian ceramics from the Mesoamerican formative village of Cuanalan, Teotihuacan Valley, Mexico

Maria Rodriguez Ceja,[1] Avto Goguitchaichvili,[1] Juan Morales,[1] Mikhail Ostrooumov,[2] Linda R. Manzanilla,[3] Bertha Aguilar Reyes,[1] and Jaime Urrutia-Fucugauchi[4]

Received 21 September 2008; revised 12 January 2009; accepted 9 February 2009; published 8 April 2009.

[1] We report a detailed archeomagnetic and micro–Raman spectroscopy investigation on pre-Columbian pottery fragments from Cuanalan (a formative village in the valley of Teotihuacan, central Mexico). Available radiocarbon ages range from 2320 ± 80 to 2060 ± 90 B.P. Continuous low-field susceptibility versus temperature curves performed in air indicate Ti-poor titanomagnetites as magnetization carriers. Few samples, however, show two ferrimagnetic phases with Curie temperatures compatible with both Ti-poor and Ti-rich titanomagnetites. Hysteresis parameter ratios fall essentially in the pseudosingle-domain region, which may indicate a mixture of multidomain and a significant amount of single-domain grains. Mineralogical composition of the Teotihuacan ceramics has been investigated using micro–Raman spectroscopy. Samples are characterized by highly heterogeneous body matrix mineralogy due to the presence of a large variety of minerals with several mineralogical phases. Observed titanomagnetite and magnetite bands shift toward higher wave numbers, confirming a reducing atmosphere and a relatively high temperature (about 800–900°C) during the ceramic production. This definitively indicates the thermoremanent origin of magnetic magnetization. Archeointensity values have been determined from 7 pottery fragments (47 samples) out of 10 (70 samples) analyzed. Anisotropy of thermoremanent magnetization and the cooling rate effect upon thermoremanent magnetization intensity acquisition have been investigated in all the samples. The mean archeointensity values obtained in this study range from 24.2 ± 3.2 to 40.0 ± 1.7 $\mu$T, and corresponding virtual axial dipole moments range from 4.8 ± 0.6 to 8.0 ± 0.4 ($10^{22}$ A m$^2$). This corresponds to a mean virtual dipole moment value of 5.9 ± 1.1 × $10^{22}$ A m$^2$, which is lower than the present-day field strength and the predicted values by global models and the latest data compilation. However, our data agree well with currently available absolute intensity values from Mesoamerica. The archeointensity values uncorrected for cooling rate and anisotropy are systematically higher than the corrected values. These uncorrected values agree with the CALS7K model, which may be biased by the fact that such corrections were not applied to most of the previous data.

**Citation:** Rodriguez Ceja, M., A. Goguitchaichvili, J. Morales, M. Ostrooumov, L. R. Manzanilla, B. Aguilar Reyes, and J. Urrutia-Fucugauchi (2009), Integrated archeomagnetic and micro–Raman spectroscopy study of pre-Columbian ceramics from the Mesoamerican formative village of Cuanalan, Teotihuacan Valley, Mexico, *J. Geophys. Res.*, *114*, B04103, doi:10.1029/2008JB006106.

## 1. Introduction

[2] Most archeological materials contain magnetic particles and acquire a remanence when cooling down below the Curie temperature after being baked, which depends on the direction and intensity of Earth's magnetic field [*Thellier and Thellier*, 1959; *Aitken*, 1990; *Chauvin et al.*, 2000; *Genevey et al.*, 2003]. The time of acquisition of the remanent magnetization can be determined by comparison of the paleomagnetic parameters of such materials from an archeological site with an already dated record of the past geomagnetic field in the same region, known as a local

[1]Laboratorio Interinstitucional de Magnetismo Natural, Instituto de Geofísica, Sede Michoacán, Universidad Nacional Autónoma de México, Morelia, Mexico.
[2]Departamento de Geología y Mineralogía, IIM, UMSNH, Morelia, Mexico.
[3]Instituto de Investigaciones Antropológicas, Universidad Nacional Autónoma de México, Mexico City, Mexico.
[4]Laboratorio de Paleomagnetismo y Paleoambientes, Instituto de Geofísica, Universidad Nacional Autónoma de México, Mexico City, Mexico.


0148-0227/09/2008JB006106$09.00

master curve. Where the past variations of Earth's magnetic field, and thus the master curves, are well established such as in Europe, archeomagnetic dating can be as precise as the most expensive radiometric dating [e.g., *Genevey and Gallet*, 2002] and does not depend on the availability of suitable carbon-bearing material.

[3] Although abundant archeological remains are available in Mexico, archeomagnetic studies are still scarce. Some early studies have been performed by *Wolfman* [1973], who reported archeomagnetic directions for archeological sites in central and eastern Mexico. The principal limitation of this pioneering work was that most of the Mexican archeological material available for archeomagnetism is not oriented. Thus, relatively few paleodirections of the geomagnetic field could be obtained. Archeointensity (AI) study has the great advantage that no oriented material is required. Such studies are now abundant for Europe [*Schnepp and Lanos*, 2005; *Gómez-Paccard et al.*, 2006] but are still scarce in America. *Bowles et al.* [2002] records for the southwestern United States and northwestern South America are quite different, which is not surprising given the substantial nondipole components of today's geomagnetic field and the distance between the regions, which exceeds the distance to the source of the field in Earth's core. Clearly, existing data are so scattered and the sites they derive from are so far one from the other in most of Mexico that they could provide at the most only very crude dating of Mesoamerican materials. Apart from some early studies on young volcanic rocks [*Nagata et al.*, 1965; *Bucha et al.*, 1970; *Lee*, 1975; *Aitken et al.*, 1991; *Gonzalez et al.*, 1997; *Morales et al.*, 2001, 2006] no serious attempts have been undertaken to determine archeointensity from Mexico.

[4] Raman spectrometry can provide diagnostic and crystal chemical information on the mineralogical phases of rocks and stone artifacts. Since nondestructive investigation is a major premise in archeometric and archeological identification, Raman spectrometric method is considered to be the most appropriate for this aim. This analytical technique is also useful as an alternative to more traditional methods of X-ray analyses such as X-ray diffraction (XRD), scanning electron microscopy (SEM), energy-dispersive spectroscopy (EDS), and electron probe microanalyzer (EPMA). Being a nondestructive microanalytical technique, Raman spectrometry is becoming increasingly important for investigations of antiquities and objects of art [*Vandenabeele et al.*, 2007]. The great advantage is also that there is no need for laborious sample preparation. In our specific case, we applied this technique in order to characterize the magnetic minerals responsible for magnetization in Cuanalan ceramics and to estimate the firing temperature.

[5] In this paper we present the results of systematic archeointensity measurements on 10 archeologically well controlled pottery fragments from Cuanalan, a formative village before the beginnings of Teotihuacan at around 300 B.C. [*Manzanilla*, 1985], the greatest classic metropolis of central Mexico. This work is part of the effort to establish an archeointensity curve for Mesoamerica. In addition, taking advantage of the recent development of micro-Raman techniques, we report for the first time a Raman spectroscopic survey of ceramic materials from the Teotihuacan Valley. The Raman microprobe is emerging as an important tool in archeological and archeometric research.

## 2. Archeological Context and Samples

[6] Teotihuacan is located some 50 km NE of Mexico City (19°41′56″N, 98°50′37″W); it was one of the largest urban developments, with a surface of 22 km$^2$. The great monumental constructions of the pyramids of the Sun, the Moon, and the Feathered Serpent, as well as the so-called Street of the Dead (names given by the Aztecs centuries after the fall of the classic city) are famous all over the world.

[7] The formative period in the Teotihuacan valley is considered to have been around 250 B.C., followed by the Tzacualli 0–100 A.D. initial phase. During the Miccaotli and Tlamimilolpa phases (100–200 A.D. and 200–350 A.D., respectively), the orthogonal city was built. The collapse of Teotihuacan occurred at about 550–600 A.D. [*Manzanilla*, 1995, 2003].

[8] The samples analyzed in the present study belong to Cuanalan, a formative village excavated by L. R. Manzanilla and M. Frangipane in the seventies [*Manzanilla*, 1985] that is located some 10 km southwest from the Teotihuacan (Figure 1). This site (400–100 B.C.) is considered to be one of the precedents of Teotihuacan. Formative 5 × 5 m houses as well as outdoor domestic facilities were excavated extensively in 1974 and 1975. All the ceramic samples, which mainly contain volcanic clay minerals, were recovered from these excavations. Radiocarbon dates associated with similar ceramic types have also been obtained for the site, particularly from carbonized wood associated with domestic refuse. Eight radiocarbon ages were dated by the Istituto di Geochimica de la Università di Roma [*Manzanilla*, 1985; *Beramendi-Orosco et al.*, 2009]. These ages vary between 2320 ± 80 and 2060 ± 90 B.P. We note that there is no direct relation between age determinations and pottery fragments analyzed. This is a common feature in archeomagnetic research. Thus, we use an average age and intensity values to discuss the intensity variation trough time.

[9] Each of 10 pottery fragments was divided in at least 7 specimens and then was "packed" into ultra pure salt (NaCl) pellets in order to treat them as standard paleomagnetic cores. In total, we obtained 70 specimens. Magnetization per unit volume of "blank" pellets ranges on the order of $10^{-5}$ A/m, whereas magnetization of typical archeomagnetic cores prepared for AI determinations ranges on the order of $10^{-2}$ to $10^{-1}$ A/m.

## 3. Experimental and Methodological Aspects

### 3.1. Viscosity Index

[10] Determination of the viscosity index [*Thellier and Thellier*, 1944; *Prévot et al.*, 1985] allows estimation of the capacity of a sample to acquire a viscous remanent magnetization and is therefore useful for obtaining information about its magnetic stability. For this purpose, we placed samples during 2 weeks with one of their axes aligned with Earth's magnetic field. After measuring the samples' magnetization before placing them in a free magnetic space ($M_d$), they were placed for another 14 days in a field-free

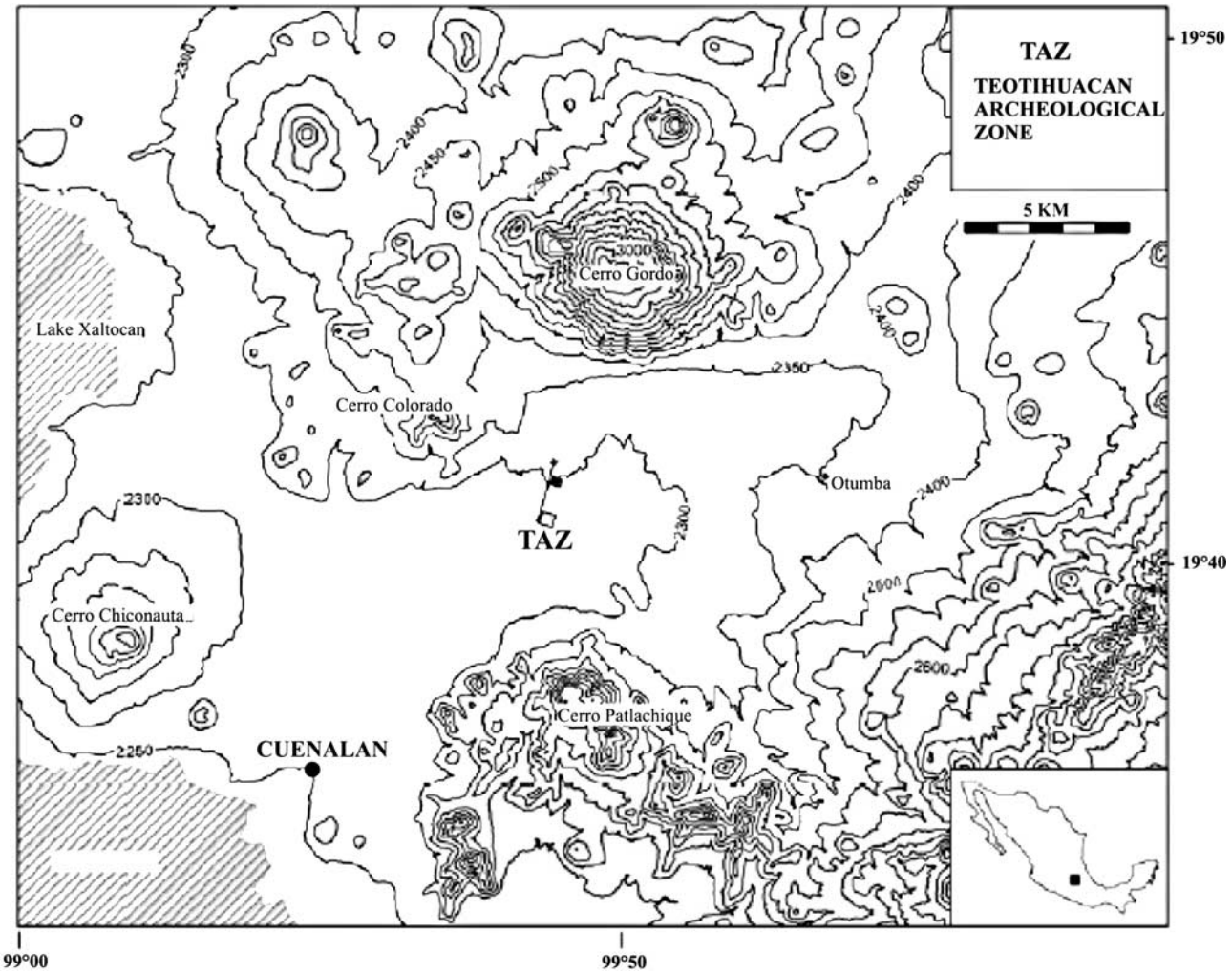


**Figure 1.** Location map of the archeological site of Cuanalan, central Mexico. TAZ means Teotihuacan archeological zone.

space, and the magnetization after being placed in a free magnetic space ($M_0$) was measured again. This allows calculation of the viscosity index $V = [(Z_d - Z_0): M_{nrm}] \times 100$, where $Z_d$ and $Z_0$ are the magnetization components of $M_d$ and $M_0$ which are parallel to the magnetizing field, respectively. $M_{nrm}$ is the intensity of natural remanent magnetization (NRM). Three samples from each fragment were subjected to these experiments, and although viscosity indexes varied between 1.5% and 10.3%, most values are lower than 5% (the average value is 2.9%). Generally speaking, the studied samples show a relatively low capacity for acquiring viscous remanent magnetization.

### 3.2. Curie Temperatures

[11] Low-field susceptibility measurements ($k$-$T$ curves) under air were carried out using a Bartington susceptibility bridge equipped with a furnace. One sample from each fragment was heated up to about 600°C at a heating rate 20°C min$^{-1}$ and then cooled at the same rate. Curie temperature was determined by *Prévot et al.*'s [1985] method.

[12] Most of the sites yield evidence for a single ferrimagnetic phase (Figure 2 and Table 1) with Curie point compatible with Ti-poor titanomagnetite. The heating and cooling curves are reasonably reversible, which attests the high thermal stability of samples. Few sites (Figure 2, sample CUAN5) yield the evidence of two ferrimagnetic phases during heating and cooling. The lower Curie points ranges between 200 and 250°C, whereas the highest one is about 580°C. Both Ti-rich and Ti-poor titanomagnetites seems to coexist in these samples. The presence of (titano)-hematite is possible, but its contribution in magnetic susceptibility seems to be negligible.

### 3.3. Hysteresis Experiments

[13] Hysteresis measurements at room temperature were performed on all samples using the alternating gradient field magnetometer ''Micromag'' apparatus in fields up to 1.4 T. The saturation remanent magnetization ($J_{rs}$), the saturation magnetization ($J_s$) and coercive force ($H_c$) were calculated after correction for the paramagnetic contribution. The coercivity of remanence ($H_{cr}$) was determined by applying progressively increasing back field after saturation. Some typical hysteresis plots are reported in Figure 3. The curves are quite symmetrical in all cases. Near the origin, no potbellied and wasp-waisted behaviors [*Tauxe et al.*, 1996] were detected, which probably reflects very restricted ranges of the opaque mineral coercivities. Judging from the

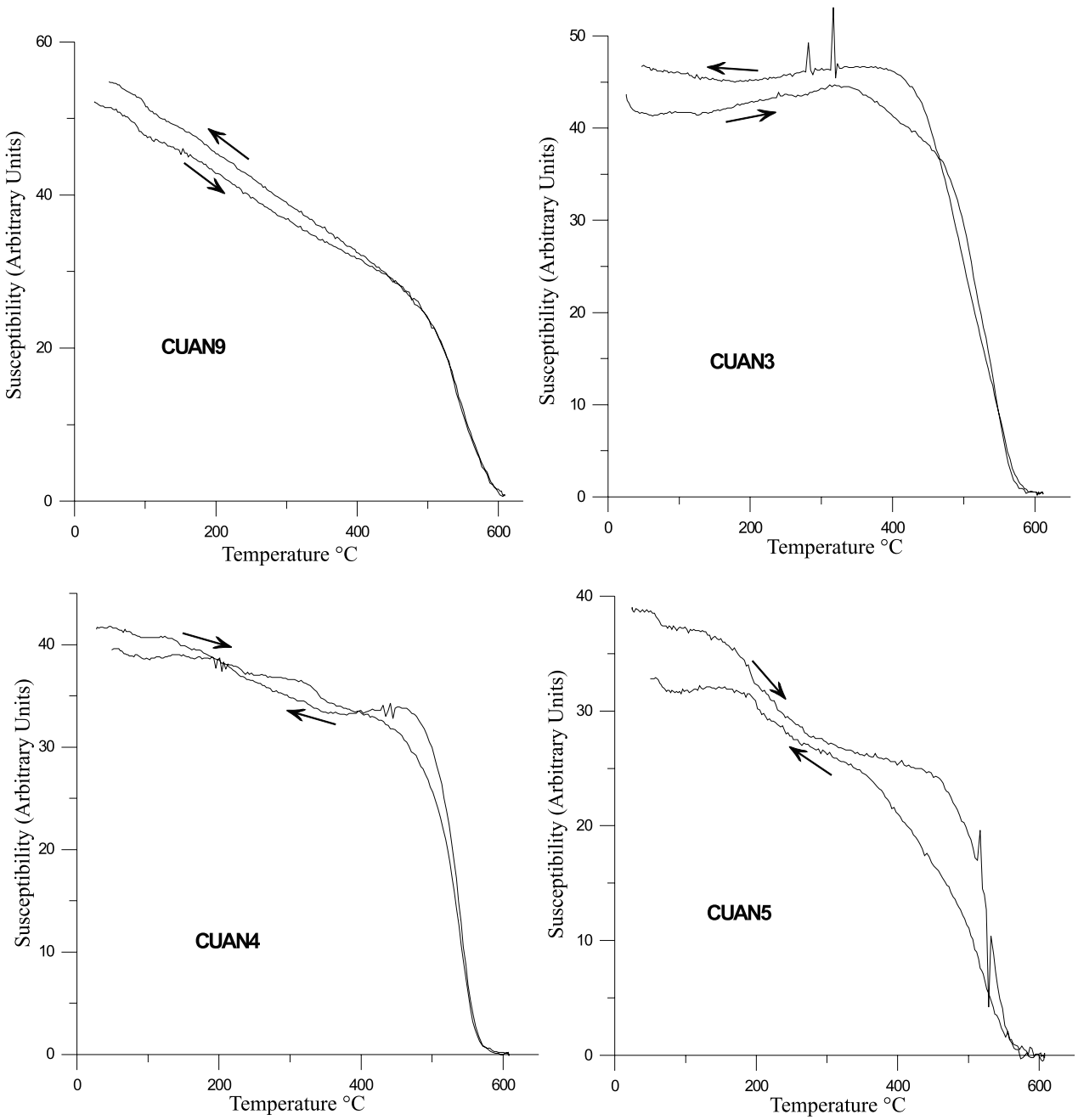


**Figure 2.** Susceptibility versus temperature (in air) curves of representative samples. The arrows indicate the heating and cooling curves.

ratios of hysteresis parameters (Figure 4 and Table 1), it seems that all samples fall in the pseudosingle-domain grain size region [*Day et al.*, 1977]. This may indicate a mixture of multidomain and a significant amount of single-domain grains [*Dunlop*, 2002]. Corresponding isothermal remanence acquisition curves were found to be very similar for all samples. Saturation is reached in moderate fields of the order of 150–200 mT, which points to some spinels (titanomagnetites) as remanence carriers.

### 3.4. Raman Spectrometry

[14] Raman spectroscopy (RS) is not a common tool in paleomagnetism in comparison to other techniques like XRD or SEM/EDS. However, RS and micro-RS (the technique used in this study) is frequently used to characterize archeological artifacts. The Raman effect is basically a process of inelastic dispersion in which the energy of the photons sent to the sample adds to or subtracts from the energies corresponding to different atomic vibrations in the analyzed sample. It can be used as an identification technique since the set of atomic vibrations is specific for each phase of a compound. The major advantage of Raman spectroscopy is that it permits the precise mineralogical identification as well as the crystal chemical information of different mineralogical phases which may coexist in ancient pottery. Raman spectroscopy is a rapid and nondestructive

**Table 1.** Summary of Rock Magnetic Experiments for Cuanalan Samples[a]

| Sample | $H_C$ (mT) | $M_{rs}$ ($\mu$A m$^2$) | $M_s$ ($\mu$A m$^2$) | $M_{rs}/M_s$ | $H_{cr}$ (mT) | $H_{cr}/H_c$ | Weight (mg) | Curie Temperature (deg C) Heating $T_{C1}$ | Heating $T_{C2}$ | Cooling $T_{c1}$ | Cooling $T_{c2}$ | Estimated Magnetic Carrier |
|---|---|---|---|---|---|---|---|---|---|---|---|---|
| CUAN 1 | 8.68 | 1.24 | 7.01 | 0.18 | 11.73 | 1.35 | 31.50 | 519 | - | 500 | - | Ti-poor Titanomagnetite |
| CUAN 2 | 9.43 | 1.17 | 8.10 | 0.14 | 19.56 | 2.07 | 31.30 | 468 | - | 453 | - | Ti-poor Titanomagnetite |
| CUAN 3 | 17.62 | 0.72 | 3.29 | 0.22 | 30.39 | 1.72 | 14.20 | 465 | - | 500 | - | Ti-poor Titanomagnetite |
| CUAN 4 | 5.10 | 0.53 | 5.21 | 0.10 | 9.86 | 1.93 | 14.80 | 515 | - | 496 | - | Ti-poor Titanomagnetite |
| CUAN 5 | 11.88 | 0.75 | 3.90 | 0.19 | 22.52 | 1.90 | 13.60 | 200 | 510 | 200 | 453 | both Ti-poor and Ti-rich Titanomagnetite |
| CUAN 6 | 7.24 | 0.88 | 5.81 | 0.15 | 20.00 | 2.76 | 11.27 | 518 | - | 460 | - | Ti-poor Titanomagnetite |
| CUAN 7 | 12.32 | 0.75 | 4.27 | 0.17 | 25.30 | 2.05 | 22.00 | 497 | - | 458 | - | Ti-poor Titanomagnetite |
| CUAN 8 | 6.88 | 0.91 | 6.29 | 0.14 | 9.04 | 1.31 | 29.00 | 205 | 458 | 315 | 430 | both Ti-poor and Ti-rich Titanomagnetite |
| CUAN 9 | 10.52 | 0.81 | 5.33 | 0.15 | 20.95 | 1.99 | 20.40 | 535 | - | 535 | - | Ti-poor Titanomagnetite |
| CUAN 10 | 10.54 | 1.15 | 6.59 | 0.17 | 19.76 | 1.87 | 32.10 | 210 | 486 | 469 | - | Ti-poor Titanomagnetite |

[a]Hysteresis parameters (the saturation remanent magnetization ($M_{rs}$), the saturation magnetization ($M_s$), the coercive force ($H_c$), and the coercivity of remanence ($H_{cr}$)) and Curie points estimation for each pottery studied.

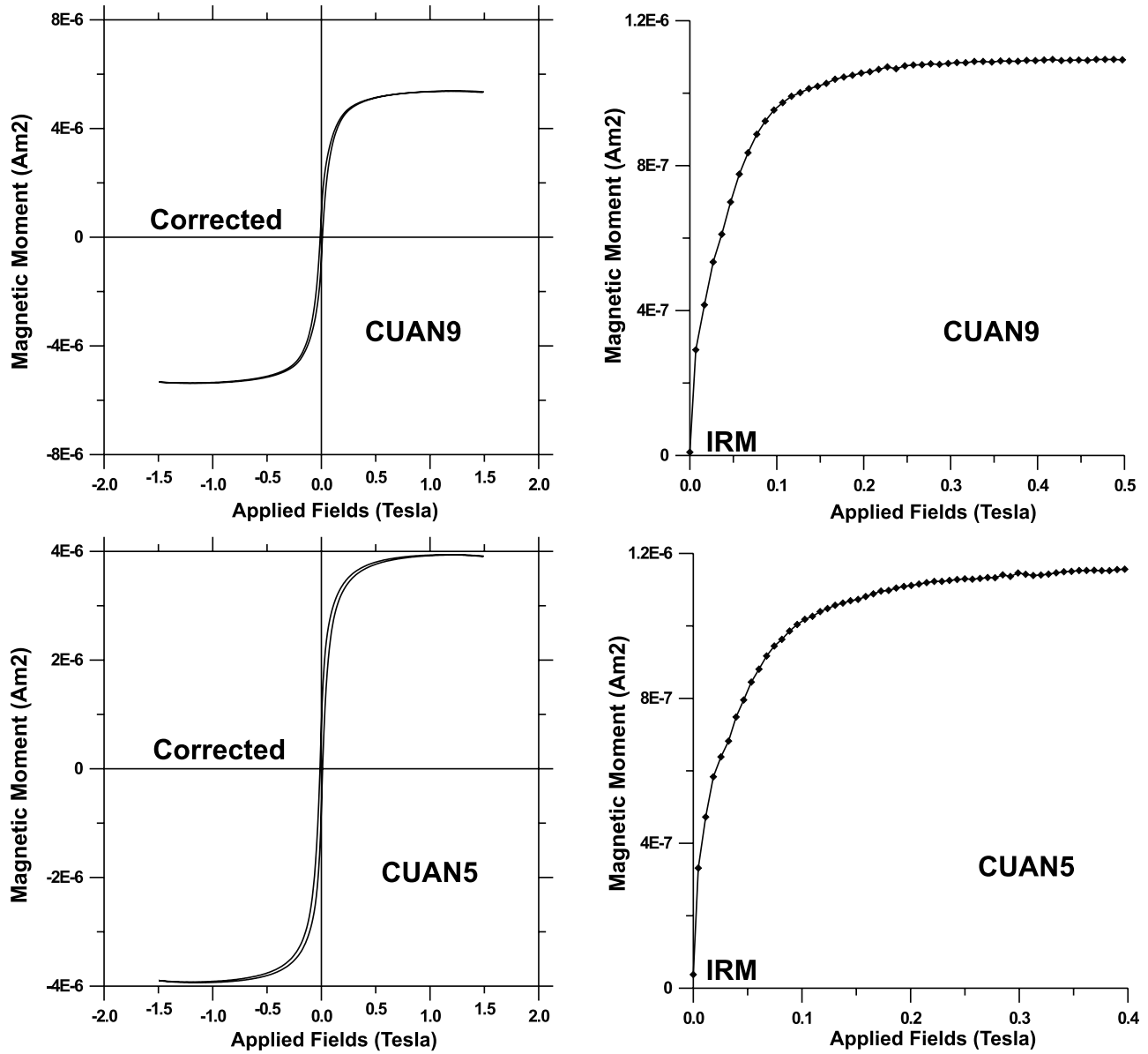


**Figure 3.** Examples of hysteresis loops and corresponding isothermal remanent magnetization (IRM) acquisition curves for representative samples.

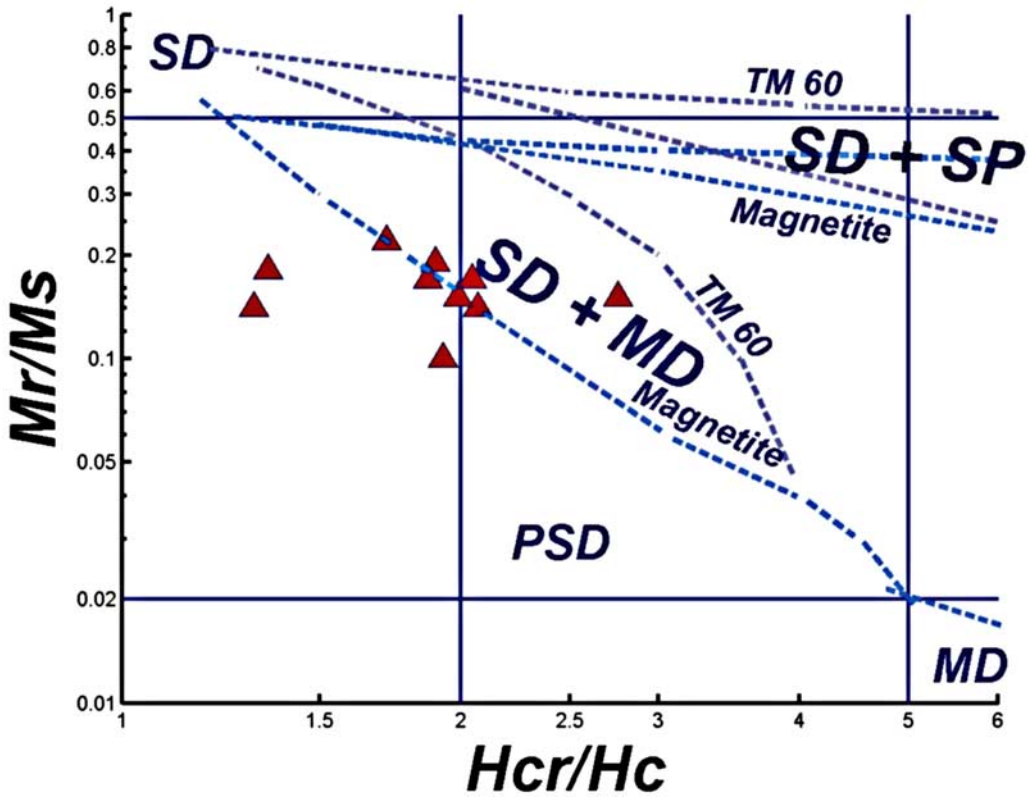


**Figure 4.** Room temperature hysteresis parameters plotted on *Dunlop*'s [2002] curve (see text for more details).

method for mineralogical analysis of ancient pottery and for the determination of firing temperatures. Moreover, it requires no sample preparation.

[15] In this study, 10 pottery fragments from Teotihuacan ceramic materials were examined with RS. Their Raman spectra were recorded with a micro-Raman spectrometer LabRam (Jobin-Yvon Horiba) using the $\lambda_L$ = 632.87 nm line of a He/Ne laser line. To avoid thermal degradation effects which affect mainly oxide minerals, the laser power on the samples was kept below 20 mW in all cases. The samples were analyzed under an Olympus microscope with 50X and 100X objectives giving 5–10 $\mu$m spatial resolution. The spectral resolution used ranged between 2 and 4 $cm^{-1}$. In order to obtain more information about the materials used in these potteries, the mineralogical composition of studied ceramic bodies was examined using so-called point-to-point micro-Raman spectrometry.

### 3.5. Archeointensity Determination

[16] *Thellier and Thellier*'s [1959] method in its modified form [*Coe*, 1967; *Coe et al.*, 1978] was used in the present study to determine absolute geomagnetic intensity. The heatings and coolings were made in air, and the laboratory field was set to 30 mT. Ten to eleven temperature steps were distributed between room temperature and 575°C. Temperature reproducibility between two heatings at the same step was in general better than 2°. The partial thermoremanent magnetization (pTRM) checks were performed after every second step throughout the whole experiment. Archeointensity data are reported on the classical NRM–thermoremanent magnetization (TRM) plot in Figure 6, and results are given in Table 2. We accepted only determinations (1) which were obtained from at least six NRM-TRM points corresponding to a NRM fraction larger than 1/3 (Table 2) and (2) which yielded a quality factor [*Coe et al.*, 1978] of about 5 or more. In a single case, we accepted the individual determination with a lower quality factor (Table 2, sample 99C044A). However, the archeointensity estimate is very close to the site mean.

[17] We define three types of behavior during Thellier experiments. Type A is characterized by important linear segments and positive pTRM checks. NRM end point directions are also linear and point to the origin. Type B samples also yielded linear Arai-Nagata curves (Figure 5) and positive control heatings, but the associated Zijderveld diagrams present two components of magnetization. Finally, NRM directions deviate strongly from the origin for type C samples, although linearity and thermal stability are maintained on NRM-TRM plots. In order to investigate whether this abnormal behavior is due to heatings under magnetic field, we thermally demagnetized sister samples in a free magnetic environment. Similarly to Thellier experiments, the orthogonal curves show clear deviation from the origin (Figure 5, sample 001B). The origin of this behavior is unclear. It may be speculated that some reheating due to firing events [*Soler-Arechalde et al.*, 2006] might produce the strong thermochemical remanent magnetization.

[18] It is well known that archeointensity strongly depends on cooling rate difference between natural and laboratory cooling conditions and on the anisotropy of

**Table 2.** Archeointensity Results Obtained for Cuanalan Potteries[a]

| | Sample | $n$ | $T_{min}-T_{max}$ | $f$ | $g$ | $q$ | $F$ | $\sigma F$ | $F_{corr}$[b] | VADM[c] | Type |
|---|---|---|---|---|---|---|---|---|---|---|---|
| CUAN 1 | 99C001A | 9 | 250–525 | 0.61 | 0.86 | 9.83 | 26.76 | 1.41 | 25.78 | 5.16 | C |
| | 99C002A | 7 | 300–525 | 0.43 | 0.79 | 6.10 | 27.80 | 1.53 | 22.80 | 4.56 | C |
| | 99C003A | 8 | 300–525 | 0.60 | 0.85 | 16.43 | 33.62 | 1.05 | 28.24 | 5.65 | C |
| | 99C004A | 8 | 250–550 | 0.57 | 0.83 | 29.02 | 36.78 | 0.60 | 28.99 | 5.80 | C |
| | 99C005A | 7 | 300–550 | 0.54 | 0.83 | 13.40 | 31.55 | 1.04 | 26.19 | 5.24 | C |
| | 99C006A | 8 | 300–550 | 0.50 | 0.85 | 6.42 | 32.43 | 2.14 | 24.84 | 4.97 | C |
| | 99C007A | 10 | 300–525 | 0.63 | 0.86 | 8.47 | 23.98 | 1.56 | 23.12 | 4.63 | C |
| Mean | | | | | | | | | 25.71 | 5.14 | |
| $\sigma$ | | | | | | | | | 2.36 | 0.47 | |
| CUAN 2 | 99C008A | 7 | 300–525 | 0.64 | 0.81 | 9.40 | 32.80 | 1.30 | 25.58 | 5.12 | A |
| | 99C009A | 9 | 300–575 | 0.79 | 0.86 | 29.13 | 31.33 | 0.73 | 24.53 | 4.91 | A |
| | 99C010A | 8 | 200–550 | 0.85 | 0.84 | 11.82 | 29.30 | 1.68 | 25.16 | 5.03 | A |
| | 99C011A | 8 | 200–550 | 0.81 | 0.85 | 14.99 | 29.10 | 1.34 | 25.46 | 5.09 | A |
| | 99C012A | 9 | 200–550 | 0.85 | 0.86 | 13.23 | 34.72 | 1.92 | 27.97 | 5.60 | A |
| | 99C013A | 10 | 200–575 | 0.83 | 0.87 | 16.30 | 32.92 | 1.47 | 26.44 | 5.29 | A |
| | 99C014A | 9 | 250–575 | 0.88 | 0.87 | 20.66 | 35.59 | 1.32 | 25.51 | 5.10 | A |
| Mean | | | | | | | | | 25.81 | 5.16 | |
| $\sigma$ | | | | | | | | | 1.11 | 0.22 | |
| CUAN 3 | 99C015A | 7 | 400–575 | 0.59 | 0.81 | 13.21 | 38.23 | 1.39 | 30.20 | 6.04 | A |
| | 99C016A | 7 | 400–575 | 0.56 | 0.80 | 7.23 | 38.58 | 2.40 | 28.54 | 5.71 | A |
| | 99C017A | 7 | 400–575 | 0.67 | 0.81 | 14.38 | 36.39 | 1.38 | 26.02 | 5.21 | A |
| | 99C018A | 7 | 400–575 | 0.66 | 0.81 | 10.40 | 37.32 | 1.90 | 26.93 | 5.39 | A |
| | 99C019A | 7 | 400–575 | 0.63 | 0.80 | 7.86 | 36.08 | 2.33 | 26.39 | 5.28 | A |
| | 99C020A | 7 | 400–575 | 0.63 | 0.79 | 6.81 | 37.02 | 2.69 | 25.10 | 5.02 | A |
| | 99C021A | 8 | 350–575 | 0.64 | 0.79 | 9.76 | 35.64 | 1.83 | 27.80 | 5.56 | A |
| Mean | | | | | | | | | 27.28 | 5.46 | |
| $\sigma$ | | | | | | | | | 1.71 | 0.34 | |
| CUAN 4 | 99C022A | 8 | 350–575 | 0.63 | 0.81 | 7.95 | 47.30 | 3.00 | 39.48 | 7.90 | A |
| | 99C023A | 8 | 350–575 | 0.74 | 0.84 | 11.77 | 53.37 | 2.81 | 38.92 | 7.79 | A |
| | 99C024A | 8 | 350–575 | 0.78 | 0.84 | 31.17 | 53.87 | 1.13 | 40.56 | 8.12 | A |
| | 99C025A | 8 | 350–575 | 0.79 | 0.83 | 15.14 | 52.46 | 2.29 | 38.12 | 7.63 | A |
| | 99C026A | 8 | 350–575 | 0.80 | 0.84 | 32.54 | 53.14 | 1.09 | 38.28 | 7.66 | A |
| | 99C027A | 8 | 350–575 | 0.74 | 0.85 | 10.37 | 54.62 | 3.28 | 42.31 | 8.47 | A |
| | 99C028A | 8 | 350–575 | 0.73 | 0.81 | 17.04 | 52.90 | 1.83 | 42.32 | 8.47 | A |
| Mean | | | | | | | | | 40.00 | 8.01 | |
| $\sigma$ | | | | | | | | | 1.78 | 0.36 | |
| CUAN 6 | 99C036A | 11 | 200–575 | 0.79 | 0.87 | 30.62 | 43.65 | 0.98 | 33.49 | 6.70 | B |
| | 99C037A | 8 | 350–575 | 0.81 | 0.86 | 9.00 | 43.49 | 3.35 | 33.02 | 6.61 | B |
| | 99C038A | 8 | 350–575 | 0.64 | 0.81 | 12.23 | 37.70 | 1.62 | 31.44 | 6.29 | B |
| | 99C039A | 8 | 350–575 | 0.82 | 0.86 | 22.10 | 40.62 | 1.31 | 34.25 | 6.85 | B |
| | 99C040A | 8 | 350–575 | 0.78 | 0.86 | 14.94 | 45.79 | 2.05 | 33.11 | 6.63 | B |
| | 99C041A | 8 | 350–575 | 0.76 | 0.85 | 16.17 | 45.46 | 1.82 | 36.77 | 7.36 | B |
| | 99C042A | 9 | 300–575 | 0.85 | 0.88 | 29.73 | 38.77 | 0.97 | 36.95 | 7.39 | B |
| Mean | | | | | | | | | 34.15 | 6.83 | |
| $\sigma$ | | | | | | | | | 2.04 | 0.41 | |
| CUAN 7 | 99C043A | 8 | 300–550 | 0.72 | 0.87 | 14.16 | 40.57 | 1.79 | 27.84 | 5.57 | C |
| | 99C044A | 6 | 350–525 | 0.46 | 0.78 | 2.74 | 40.05 | 5.29 | 31.22 | 6.25 | C |
| | 99C045A | 7 | 350–550 | 0.62 | 0.86 | 9.98 | 35.76 | 1.90 | 22.13 | 4.43 | C |
| | 99C046A | 7 | 350–550 | 0.72 | 0.86 | 17.96 | 39.04 | 1.35 | 32.01 | 6.41 | C |
| | 99C047A | 8 | 350–575 | 0.73 | 0.68 | 5.78 | 41.04 | 3.54 | 35.76 | 7.16 | C |
| Mean | | | | | | | | | 29.79 | 5.96 | |
| $\sigma$ | | | | | | | | | 5.13 | 1.03 | |
| CUAN 8 | 99C050A | 9 | 20–550 | 0.64 | 0.71 | 21.00 | 33.53 | 0.73 | 28.43 | 5.69 | A |
| | 99C051A | 9 | 20–550 | 0.63 | 0.66 | 11.40 | 24.74 | 0.91 | 21.27 | 4.26 | A |
| | 99C052A | 8 | 20–475 | 0.29 | 0.82 | 3.30 | 24.72 | 1.73 | 21.88 | 4.38 | A |
| | 99C053A | 9 | 20–475 | 0.68 | 0.70 | 14.10 | 30.62 | 1.03 | 23.64 | 4.73 | A |
| | 99C054A | 8 | 200–550 | 0.62 | 0.63 | 7.50 | 27.47 | 1.45 | 21.13 | 4.23 | A |
| | 99C055A | 9 | 200–575 | 0.87 | 0.77 | 28.10 | 35.76 | 0.85 | 28.88 | 5.78 | A |
| | 99C056A | 8 | 200–550 | 0.66 | 0.69 | 10.80 | 31.04 | 1.31 | 24.15 | 4.83 | A |
| Mean | | | | | | | | | 24.20 | 4.84 | |
| $\sigma$ | | | | | | | | | 3.25 | 0.65 | |

[a]Here, $n$ is the number of heating steps used to determine intensity; $T_{min}-T_{max}$ is the temperature interval of intensity determination; $f$ is the fraction of extrapolated NRM used for intensity determination; $g$ is the gap factor; $q$ is the quality factor as defined by *Coe et al.* [1978]; $F$ is raw archeointensity value, i.e., before cooling rate and anisotropy corrections; $F$corr is an archeointensity value after corrections; VADM is the virtual axial dipole moment.
[b]$F$corr site mean is 29.56, and $\sigma$ is 5.67.
[c]VADM site mean is 5.92, and $\sigma$ is 1.14.

thermoremanent magnetization [*Chauvin et al.*, 2000; *Genevey and Gallet*, 2002; *Le Goff and Gallet*, 2004]. Cooling rate dependence of TRM is investigated following a modified procedure described by *Chauvin et al.* [2000]. TRM gained during the last step of the Thellier experiment (for instance, at 575°C) is designated as TRM1. At the same temperature, a new TRM (TRM2) is given to all samples using a longer cooling time (~10 h). Finally, a third TRM

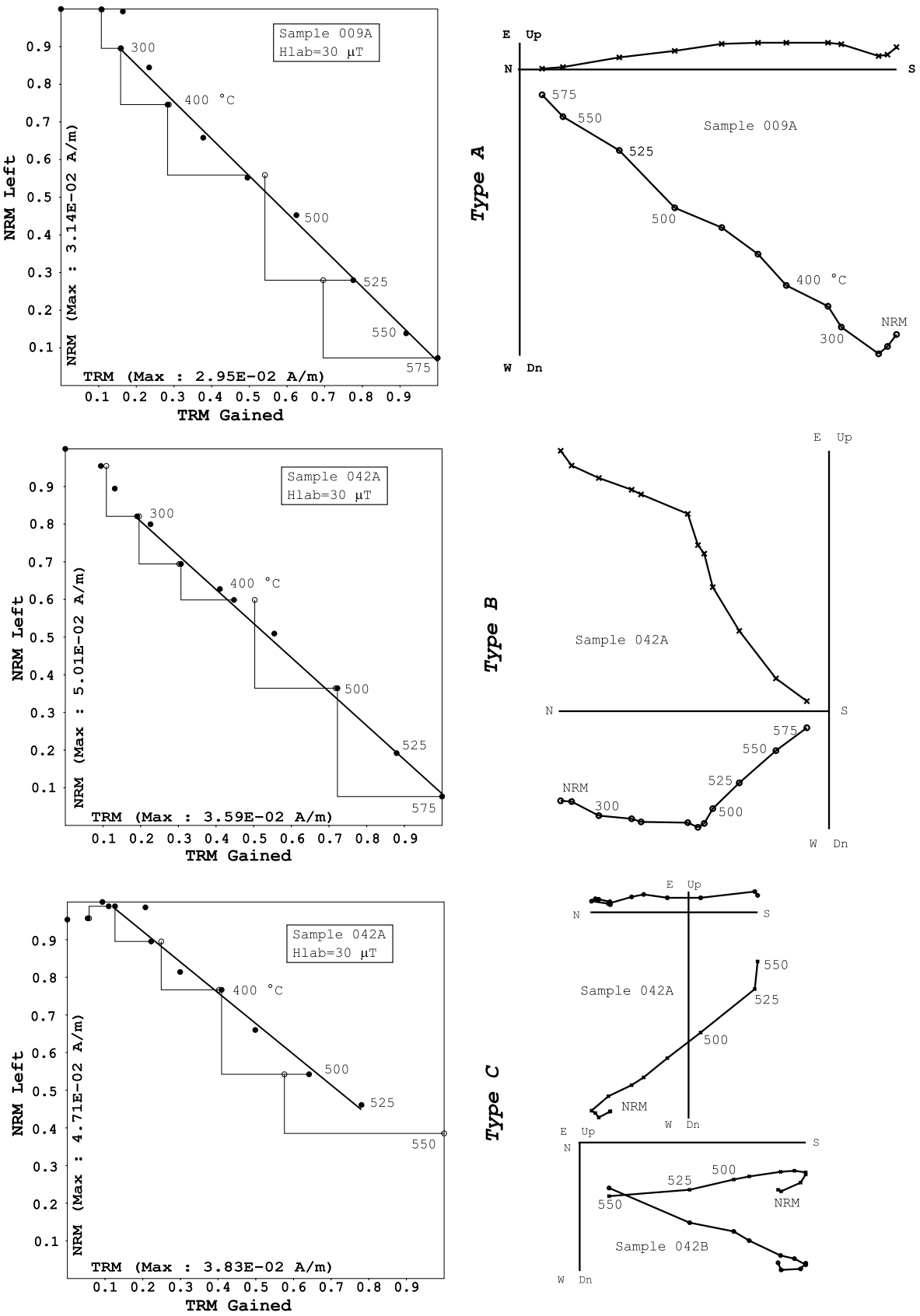


**Figure 5.** (left) Representative NRM-TRM plots and (right) associated orthogonal vector demagnetization diagrams for Cuanalan samples. In the NRM-TRM plots, open circles refer to the pTRM checks. In the orthogonal diagrams, the numbers refer to the temperatures in °C, open circles show projections into the horizontal plane, and the crosses show projections into the vertical plane.

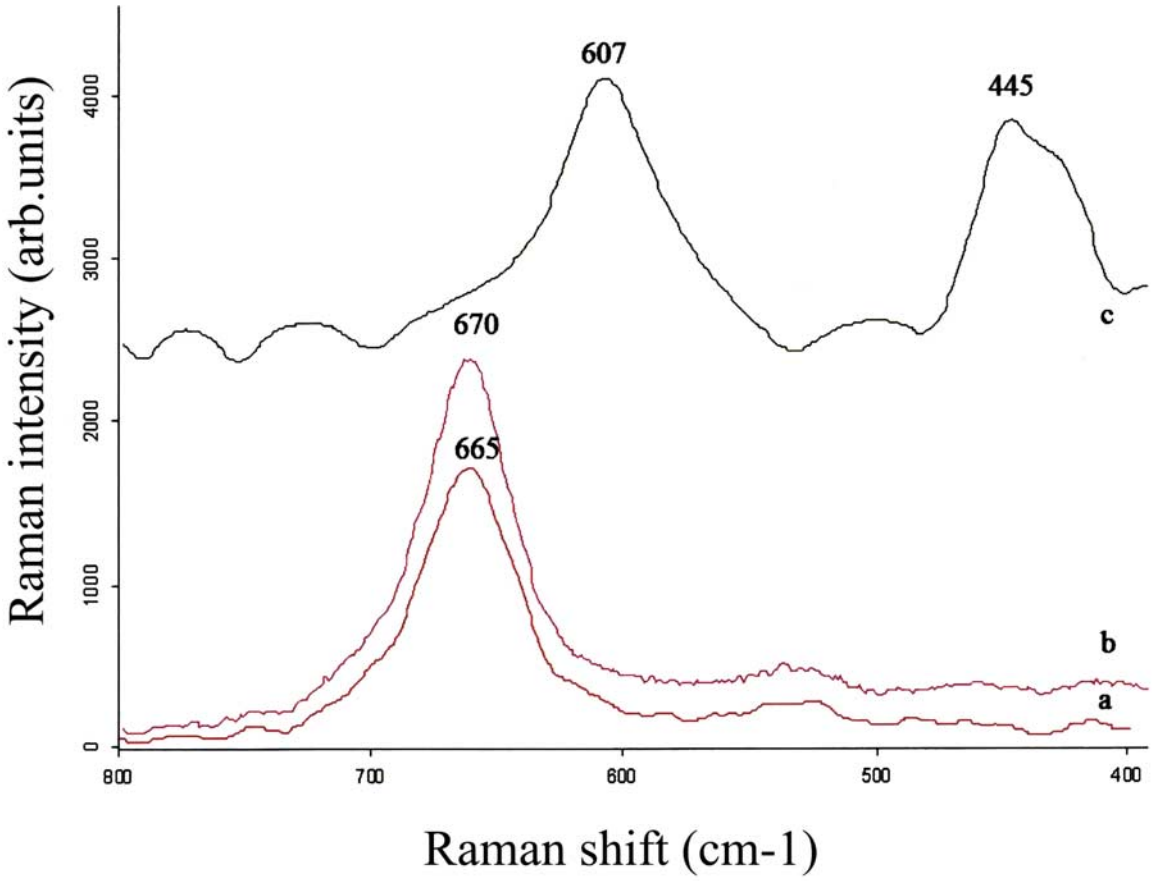


**Figure 6.** Raman spectra of magnetite (curve a), Ti-magnetite (curve b), and rutile (curve c). Note the major peak position shift (665 to 670 $cm^{-1}$) as a function of magnetite chemistry that is caused by the substitutional solid solution among Fe and Ti.

(TRM3) is created using the same cooling time (of about 45 min) as for TRM1. The effect of cooling rate upon TRM intensity is estimated by calculating the percent variation between the intensity acquired during a short and a long cooling time (TRM1 and TRM2). Any change in TRM acquisition capacity caused by alteration during laboratory heating is estimated by means of the percent variation between the intensity acquired during the same cooling time (TRM1 and TRM3).

[19] Anisotropy of TRM is determined following the procedure of *McCabe et al.* [1985]. The specimens are given a TRM along six axial directions ($+X$, $+Y$, $+Z$, $-X$, $-Y$, and $-Z$) by cooling them from 600°C to room temperature in the known magnetic field. A zero-field demagnetization step between each TRM step is used as a baseline. Calculation of the TRM anisotropy tensor then allows correction of results of the archeointensity determination.

## 4. Main Results and Discussion

[20] Rock magnetic experiments which included viscosity index, low-field susceptibility versus temperature, hysteresis, and isothermal remanence measurements indicate that the main magnetic carrier is Ti-poor titanomagnetite. In a few cases, both Ti-rich and Ti-poor titanomagnetites seem to coexist. The contribution of (titano)hematites seems to be minor. These magnetic minerals seem to be composed of mixtures of multidomain and significant amount of single-domain grains.

[21] The Raman spectra obtained from selected areas of the rough fragments from the Teotihuacan ceramic materials show that these samples are characterized by the highly heterogeneous body matrix mineralogy due to the presence of a large variety of minerals such as feldspars (alkali polymorph and plagioclase), diopside, magnetite and Ti-magnetite, and one titanium oxide, rutile. The Raman spectrum of a confirmed diopside has been recorded in the range 100–1500 $cm^{-1}$. This pyroxene starts to crystallize in calcareous clays at a temperature near to 800–900°C [*Colomban*, 2005]. Thus, the magnetic remanence recorded in Cuanalan samples is definitively of thermoremanent origin.

[22] Figure 6 (curve a) shows an example of a magnetite spectrum acquired in some inclusions which have been found in ceramic materials. The internal vibration of the $Fe^{3+}O_6$ octahedron has been assigned as the major contributor to the main Raman broadband of magnetite detecting around 662–665 $cm^{-1}$ which is typical of the inverse spinel structures. It is very important to stress that some Raman spectra of magnetite are characterized by a main peak that shifts toward high wave numbers (670–675 $cm^{-1}$). This phenomenon occurs because there is the solid solution in

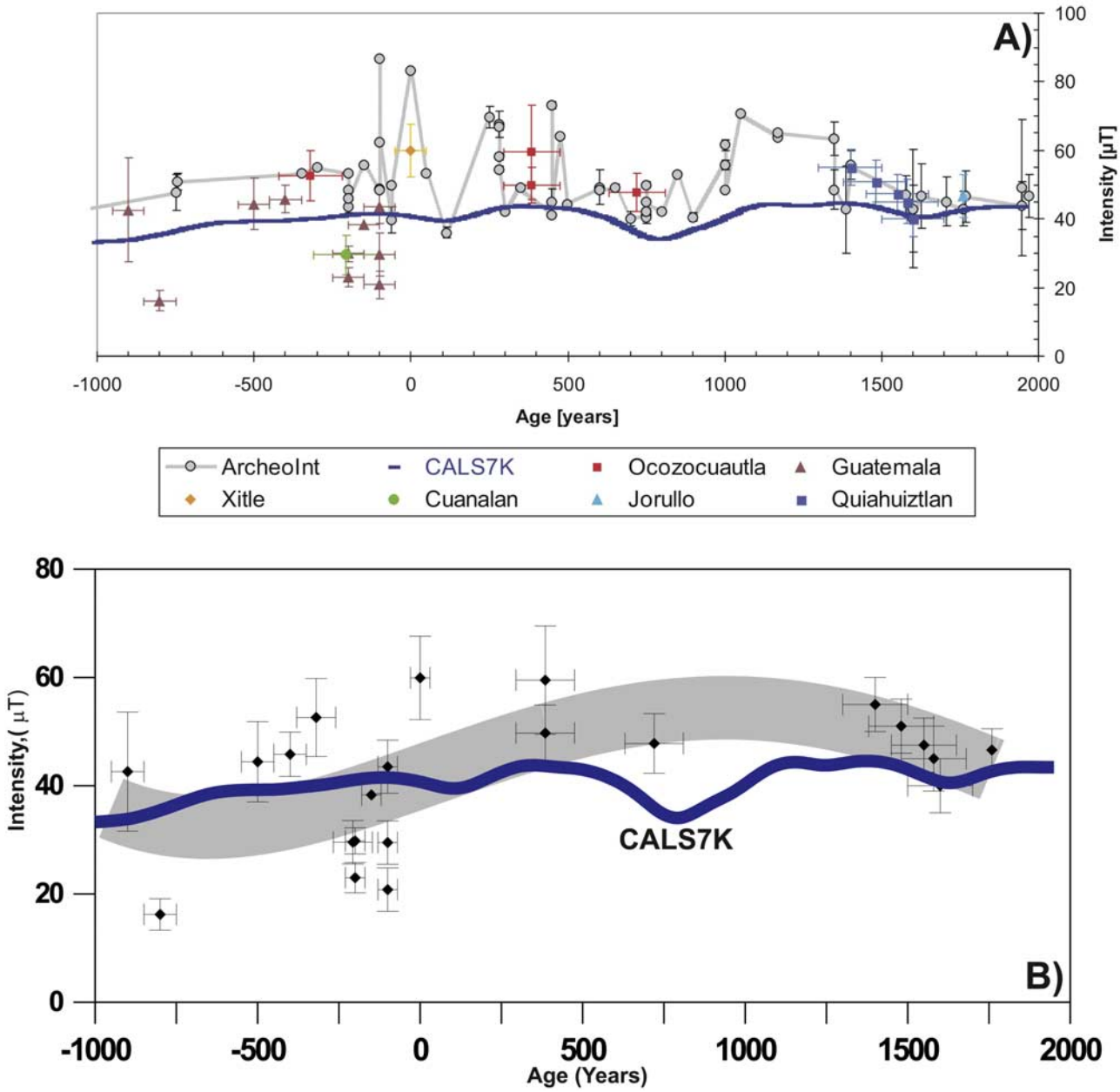


**Figure 7.** (a) Currently available absolute intensity data from Mesoamerica derived from archeological artifacts and historic lava flows. Also shown is the curve obtained using a worldwide archeointensity database reduced to Mexico City [*Genevey et al.*, 2008]. The blue line represents model prediction from CALS7K [*Korte and Constable*, 2005]. Measurement data sources are as follows: Xitle from *Morales et al.* [2006], Ocozocuautla from *Morales et al.* [2009], Jorullo from *Gratton et al.* [2005], Guatemala from L. Alva-Valdivia (unpublished data, personal communication, 2009), and Quiahuiztlan from *López-Téllez et al.* [2007]. (b) A general tendency of available archeointensity data distribution using simple polynomial adjustment compared to the CALS7K model.

the magnetite-ulvöspinel structures where the vibrations of $Ti^{4+}O_6$ and $Fe^{3+}O_6$ octahedra control their Raman spectra features (Figure 6, curve b). When forming Ti-magnetite, the main Raman peak is shifted upward, consistent with the increase of $Ti^{4+}O_6$ fractions in their structures. The Raman spectrum of rutile is also shown in Figure 6 (curve c), and it agrees well with previously published spectra which exhibit two prominent bands (typical doublet) of 445 and ~607 $cm^{-1}$ (M. Ostrooumov et al., FT-Raman and infrared reflection spectrometry of minerals and gems, available at http://www.geocities.com/ostroum, 2006).

[23] Forty-seven samples out of seventy analyzed yield reliable absolute intensity determinations; twenty-eight of them correspond to type A (Table 2), seven are type B, and the remaining twelve samples yield type C determinations. For these samples the NRM fraction $f$ used for determination ranges between 0.29 and 0.88, and the quality factor $q$ ranges from 2.7 to 32.5, being generally greater than 5. The

cooling rate and anisotropy corrections significantly reduced the standard deviation of the mean intensities, suggesting the importance of such a correction in this kind of study. The fragment-mean paleointensity values obtained in this study range from 24.2 ± 3.2 to 40.0 ± 1.7 $\mu$T, with corresponding virtual axial dipole moments ranging from 4.8 ± 0.6 to 8.0 ± 0.4 ($10^{22}$ A $m^2$). This corresponds to mean virtual dipole moment value of 5.9 ± 1.1 × $10^{22}$ A $m^2$, which is lower than present-day field strength (Figure 7). Exclusion of type C determinations does not significantly change the global mean.

[24] The Cuanalan mean archeointensity is shown in Figure 7a together with other selected mean intensities currently available from Mesoamerica. Also shown are the curve derived from the CALS7K global model [*Korte and Constable*, 2005] and data retrieved from a worldwide archeointensity database (data reduced to Mexico City [*Genevey et al.*, 2008]). The robust mean archeointensity obtained in the present study differs from predicted absolute intensities retrieved from the CALS7K global model and the latest archeointensity compilation data ArcheoInt, yielding significantly lower values (Figure 7b). However, our data agree well with currently available absolute intensity values from Mesoamerica. The archeoinintensity values not corrected for cooling rate and anisotropy are systematically higher than the corrected values. These uncorrected values agree with the CALS7K model, which may be biased by the fact that such corrections were not applied to most of the previous data.

[25] **Acknowledgments.** We thank Annick Chauvin and Pierrick Roperch for their great help during the measurements at the paleomagnetic laboratory of the University of Rennes, France. Financial support was provided by CONACYT project 54957. The Cuanalan excavation (under L. R. Manzanilla's and M. Frangipane's Palaeoethnological Project of the Valley of Teotihuacan (PPVT)) was funded by the Università di Roma "La Sapienza" and the Instituto Nacional de Antropología e Historia-Mexico. B.A. acknowledges the financial support given by UNAM-PAPIIT IN113009.

## References

Aitken, M. J. (1990), *Science-Based Dating in Archaeology*, pp. 225–259, Longman, New York.

Aitken, M. J., L. J. Pesonen, and M. Leino (1991), The Thellier paleointensity technique: Minisamples versus standard size, *J. Geomagn. Geoelectr.*, *43*, 325–331.

Beramendi-Orosco, L., G. Gonzalez-Hernandez, J. Urrutia-Fucugauchi, L. Manzanilla, A. Soler-Arechalde, A. Goguitchaishvili, and N. Jarboe (2009), High resolution chronology for the Mesoamerican urban center of Teotihuacan derived from Bayesian statistics of radiocarbon and archaeological data, *Quat. Res.*, *71*, 99–107, doi:10.1016/j.yqres.2008.10.003.

Bowles, J., J. Gee, J. Hildebrand, and L. Tauxe (2002), Archeomagnetic intensity results from California and Ecuador: Evaluation of regional data, *Earth Planet. Sci. Lett.*, *203*, 967–981, doi:10.1016/S0012-821X(02)00927-5.

Bucha, V., R. E. Tylor, R. Berger, and E. W. Haury (1970), Geomagnetic intensity: Changes during the past 3000 years in the Western Hemisphere, *Science*, *168*, 111–114, doi:10.1126/science.168.3927.111.

Chauvin, A., Y. Garcia, P. Lanos, and F. Laubenheimer (2000), Paleointensity of the geomagnetic field recovered on archaeomagnetic sites from France, *Phys. Earth Planet. Inter.*, *120*, 111–136, doi:10.1016/S0031-9201(00)00148-5.

Coe, R. S. (1967), Paleo-intensities of the Earth's magnetic field determined from Tertiary and Quaternary rocks, *J. Geophys. Res.*, *72*(12), 3247–3262, doi:10.1029/JZ072i012p03247.

Coe, R. S., S. Grommé, and E. A. Mankinen (1978), Geomagnetic paleointensities from radiocarbon-dated lava flows on Hawaii and the question of the Pacific nondipole low, *J. Geophys. Res.*, *83*(B4), 1740–1756, doi:10.1029/JB083iB04p01740.

Colomban, P. (2005), Case study: Glasses, glazes and ceramics—Recognition of ancient technology from the Raman spectra, in *Raman Spectroscopy in Archaeology and Art History*, edited by H. G. M. Edwards and J. M. Chalmers, chap. 13, pp. 192–206, R. Soc. of Chem., Cambridge, U. K.

Day, R., M. Fuller, and V. A. Schmidt (1977), Hysteresis properties of titanomagnetites: Grain-size and compositional dependence, *Phys. Earth Planet. Inter.*, *13*, 206–267.

Dunlop, D. J. (2002), Theory and applications of the day plot ($M_{rs}/M_s$ versus $H_{cr}/H_c$): 1. Theorical curves and tests using titanomagnetite data, *J. Geophys. Res.*, *107*(B3), 2056, doi:10.1029/2001JB000486.

Genevey, A., and Y. Gallet (2002), Intensity of the geomagnetic field in western Europe over the past 2000 years: New data from ancient French pottery, *J. Geophys. Res.*, *107*(B11), 2285, doi:10.1029/2001JB000701.

Genevey, A., Y. Gallet, and J.-C. Margueron (2003), Eight thousand years of geomagnetic field intensity variations in the eastern Mediterranean, *J. Geophys. Res.*, *108*(B5), 2228, doi:10.1029/2001JB001612.

Genevey, A., Y. Gallet, C. G. Constable, M. Korte, and G. Hulot (2008), ArcheoInt: An upgraded compilation of geomagnetic field intensity data for the past ten millennia and its application to the recovery of the past dipole moment, *Geochem. Geophys. Geosyst.*, *9*, Q04038, doi:10.1029/2007GC001881.

Gómez-Paccard, M., A. Chauvin, P. Lanos, J. Thiriot, and P. Jimenez-Castillo (2006), Archeomagnetic study of seven contemporaneous kilns from Murcia (Spain), *Phys. Earth Planet. Inter.*, *157*, 16–32, doi:10.1016/j.pepi.2006.03.001.

Gonzalez, S., G. Sherwood, H. Böhnel, and E. Schnepp (1997), Paleosecular variation in central Mexico over the last 30,000 years: The record from lavas, *Geophys. J. Int.*, *130*, 201–219, doi:10.1111/j.1365-246X.1997.tb00999.x.

Gratton, M., A. Goguitchaichvili, G. Conte, J. Urrutia, and J. Shaw (2005), Microwave paleointensity study of Jorullo Volcano (central Mexico), *Geophys. J. Int.*, *161*, 627–634, doi:10.1111/j.1365-246X.2005.02619.x.

Korte, M., and C. G. Constable (2005), Continuous geomagnetic field models for the past 7 millennia: 2. CALS7K, *Geochem. Geophys. Geosyst.*, *6*, Q02H16, doi:10.1029/2004GC000801.

Le Goff, M., and Y. Gallet (2004), A new three-axis vibrating sample magnetometer for continuous high-temperature magnetization measurements: Applications to paleo- and archeo-intensity determinations, *Earth Planet. Sci. Lett.*, *229*, 31–43, doi:10.1016/j.epsl.2004.10.025.

Lee, S. S. (1975), Secular variation of the intensity of the geomagnetic field during the past 3,000 years in North, Central and South America, Ph.D. thesis, Univ. of Okla., Norman.

López-Téllez, J. M., B. Aguilar-Reyes, J. Morales, A. Goguitchaichvili, M. Calvo-Rather, and J. Urrutia-Fucugauchi (2007), Magnetic characteristics and archeointensity determination on some Mesoamerican pre-Columbian potteries: Case study of Quiahuiztlan archeological site (Veracruz, Gulf of Mexico, 900–1521 A.D.), *Geofis. Int.*, *47*, 11–18.

Manzanilla, L. (1985), El sitio de Cuanalan en el marco de las comunidades pre-urbanas del Valle de Teotihuacan, in *Mesoamérica y el Centro de México*, edited by J. Monjarás-Ruiz, R. Brambila, and E. Pérez Rocha, pp. 133–178, Inst. Nac. de Antropol. e Hist., Mexico City.

Manzanilla, L. (1995), La zona del Altiplano central en el clásico, historia antigua de México, report, pp. 139–173, Univ. Nac. Auton. Mex., Mexico City.

Manzanilla, L. (2003), El proceso de abandono de Teotihuacan y su reocupación por grupos epiclásicos, CEMCA México, *Trace*, *43*, 70–76.

McCabe, C., M. Jackson, and B. Ellwood (1985), Magnetic anisotropy in the Trenton limestone: Results of a new technique, anisotropy of anhysteretic susceptibility, *Geophys. Res. Lett.*, *12*, 333–336, doi:10.1029/GL012i006p00333.

Morales, J., A. Goguitchaichvili, and J. Urrutia-Fucugauchi (2001), A rock-magnetic and paleointensity study of some Mexican volcanic lava flows during the latest Pleistocene to the Holocene, *Earth Planets Space*, *53*(9), 893–902.

Morales, J., L. M. Alva-Valdivia, A. Goguitchaichvili, and J. Urrutia-Fucugauchi (2006), Cooling rate corrected paleointensities from the Xitle lava flow: Evaluation of within-site scatter for single spot-reading cooling units, *Earth Planets Space*, *58*(10), 1341–1347.

Morales, J., A. Goguitchaichvili, G. Acosta, T. González-Morán, L. Alva-Valdivia, J. Robles-Camacho, and M. Hernández-Bernal (2009), Magnetic properties and archeointensity determination on pre-Columbian pottery from Chiapas, Mesoamerica, *Earth Planets Space*, *61*(1), 83–91.

Nagata, T., K. Kobayashi, and E. J. Schwarz (1965), Archeomagnetic intensity studies of South and Central America, *J. Geomagn. Geoelectr.*, *17*, 399–405.

Prévot, M., E. A. Mankinen, R. S. Coe, and S. Grommé (1985), The Steens Mountain (Oregon) geomagnetic polarity transition: 2. Field intensity variations and discussion of reversal models, *J. Geophys. Res.*, *90*(B12), 10,417–10,448, doi:10.1029/JB090iB12p10417.

Schnepp, E., and P. Lanos (2005), Archaeomagnetic secular variation in Germany during the past 2500 years, *Geophys. J. Int.*, *163*, 479–490, doi:10.1111/j.1365-246X.2005.02734.x.

Soler-Arechalde, A. M., F. Sanchez, M. Rodriguez, C. Caballero-Miranda, A. Goguitchaishvili, J. Urrutia-Fucugauchi, L. Manzanilla, and D. Tarling (2006), Archaeomagnetic investigation of some oriented pre-Columbian lime plasters from Teotihuacan, Mesoamerica, *Earth Planets Space*, *58*(10), 1433–1439.

Tauxe, L., T. A. T. Mullender, and T. Pick (1996), Pot-bellies, wasp-waists and superparamagnetism in magnetic hysteresis, *J. Geophys. Res.*, *101*(B1), 571–583.

Thellier, E., and O. Thellier (1944), Recherches géomagnétiques sur les coulées volcaniques d'Auvergne, *Ann. Geophys.*, *1*, 37–52.

Thellier, E., and O. Thellier (1959), Sur l'intensité du champ magnétique terrestre dans le passé historique et géologique, *Ann. Geophys.*, *15*, 285–376.

Vandenabeele, P., H. Edwards, and L. Moens (2007), A decade of Raman spectroscopy in art and archaeology, *Chem. Rev.*, *107*(3), 675–686, doi:10.1021/cr068036i.

Wolfman, D. (1973), A re-evaluation of Mesoamerican chronology: A.D. 1–1200, Ph.D. thesis, Univ. of Colo., Denver.

B. Aguilar Reyes, A. Goguitchaichvili, J. Morales, and M. Rodriguez Ceja, Laboratorio Interinstitucional de Magnetismo Natural, Instituto de Geofísica, Sede Michoacán, Universidad Nacional Autónoma de México, Campus Morelia, Morelia, Michoacán 58089, México. (avto@geofisica.unam.mx)

L. R. Manzanilla, Instituto de Investigaciones Antropológicas, Universidad Nacional Autónoma de México, Ciudad de México, D.F. 04510, México.

M. Ostrooumov, Departamento de Geología y Mineralogía, IIM, UMSNH, Morelia, Michoacán 58087, México.

J. Urrutia-Fucugauchi, Laboratorio de Paleomagnetismo y Paleoambientes, Instituto de Geofísica, Universidad Nacional Autónoma de México, Ciudad de México, D.F. 04510, México.